Study of Surface Acoustic Wave Transmission Property With Different Interdigital Transducer Materials

You Zhou, Sezin Sayin, and Mona Zaghloul

Abstract – Today, surface acoustic wave (SAW) technology has been widely used in wireless communication, radio-frequency identification tagging, biomedical sensors, drug delivery, small particle manipulation, electronic and optical property control, and many other areas. SAW devices are usually designed on a piezoelectric substrate. It is essential to design a SAW device carefully with parameters such as delay line distance, interdigital transducer (IDT) size, center working frequency, and piezoelectric coefficients of the substrate. The choice of the material of IDTs can also affect the performance of a SAW device. In this article, we report on the use of different IDT materials to change the transmission property S_{21} and the center working frequency f_0 of a SAW device. The results show that the center frequency of a SAW device varies with different IDT materials. In addition, using low-resistivity IDT material can reduce the insertion loss of SAW devices.

1. Introduction

The surface acoustic wave (SAW) has numerous applications in different fields. For example, it has been used in communications [1], pressure sensors [2], temperature sensors [3], glucose biosensors [4], electronic and optical property control [5, 6], cell manipulation [7], drug delivery [8], and two-dimensional material property enhancement [9].SAW devices have the advantage of having a small size, being of low cost and easy to fabricate, having low power consumption, and being used as passive devices [10]. The generation of SAW results from applying AC voltage on a piezoelectric substrate through input interdigital transducers (IDTs). As shown in Figure 1, IDTs are fabricated on piezoelectric material, such as $LiNbO_3$. The input IDTs convert electrical energy into mechanical energy, while the output IDTs convert mechanical energy into electrical energy. The SAW that is generated by input IDTs can propagate along the delay line and reach the output IDTs. The electrode resistance of IDTs can affect the properties of the propagating SAW [11]. In this work, we explore how different IDT materials affect the transmission property and center working frequency of SAW devices.

Manuscript received 24 December 2021.

You Zhou, Sezin Sayin, and Mona Zaghloul are with George Washington University, 800 22nd Street, Washington, DC 20052, USA; e-mail: yzhou57@gwu.edu, sezinsayin@email.gwu.edu, zaghloul@gwu.edu.

Acknowledgment: This research was funded by U.S. National Science Foundation (NSF), award number 2033044. Award Title is "Enhancement of Piezoelectric Properties in two-dimensional materials and its application"

2. Theoretical Background

The governing equation for the generation of SAWs is

$$v_{SAW} = \lambda \times f_0 \tag{1}$$

where v_{SAW}, λ, and f_0 are the wave acoustic velocity through the piezoelectric material, the period of the IDTs (which is also the wavelength of the SAW), and the applied AC frequency, respectively. The width w of each finger of the IDTs is a quarter of the wavelength λ [8]. In this work, the finger width is chosen as 4 μm. Then the wavelength can be calculated as

$$\lambda = 4 \times w = 4 \times 4\ \mu\text{m} = 16\ \mu\text{m} \tag{2}$$

The v_{SAW} is 3996 m/s for a 128-degree Y-X cut $LiNbO_3$ piezoelectric substrate. The f_0 can be calculated as 249.75 MHz.

A Mason-equivalent circuit is selected to model the device [12]. A three-port network is used to represent each IDT, and the circuit is shown in Figure 2. Note that the acoustic reflections from IDT discontinuities cannot be neglected because this device has a thick electrode film. The Mason-equivalent circuit approximation works only for very low $h/\lambda \ll \sim 1\%$, where h stands for electrode thickness. In this work, electrodes of different materials of 200 nm thickness are fabricated as the IDTs on the 128-degree Y-X cut $LiNbO_3$ piezoelectric substrate. The h/λ ratio is $h/\lambda = 0.2\ \mu\text{m}/16\ \mu\text{m} = 0.0125 > 0.01$. Thus, this Mason-equivalent circuit is not very accurate to represent SAW

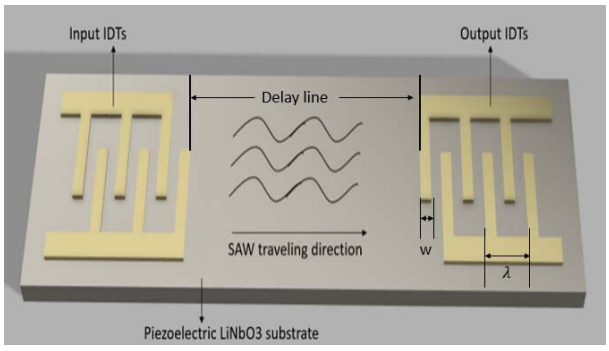

Figure 1. Typical structure of a SAW device.

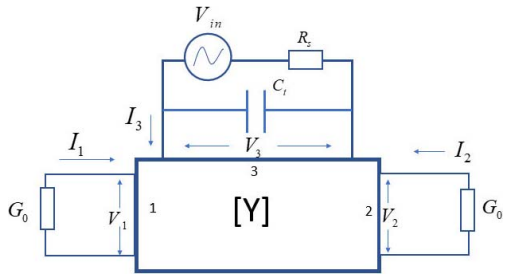

Figure 2. Three-port equivalent admittance network representation of an IDT, where G_0 is the characteristic electrical admittance of a one-period IDT, C_t is the total capacitance of the IDT fingers, and N is the number of pairs. They obey the following equations:

$$\theta = 2\pi(f/f_0), Y_{11} = -jG_0\cot(N\theta), Y_{12} = jG_0\csc(N\theta)$$
$$Y_{13} = -jG_0\tan(\theta/4), Y_{33} = j\omega C_t + j4NG_0\tan(\theta/4)$$
$$Y_{21} = Y_{12}, Y_{22} = Y_{11}, Y_{31} = Y_{13}, Y_{32} = -Y_{13}$$

devices. Our previous work shows a modified Mason-equivalent circuit and a detailed description in [10].

The SAW travels through a region that is called a delay line and then reaches the output IDTs. The equivalent circuit for the SAW delay line is illustrated in Figure 3 by applying the same method that models the IDTs [10].

The transfer function $H(f)$ of the input and output voltage is shown in (3)–(6) [10]:

$$G_a(f) = \mathrm{Re}\left[\frac{I_3}{V_3}\right] = \mathrm{Re}\left[2\frac{(-jG_{0m}\tanh(\alpha + j\theta_m))^2}{G_0 + {Y_{11}}^f - {Y_{12}}^f}\right] \quad (3)$$

$$y_{aa} = y_{bb} = G_a(f) + j2\pi f C_t \quad (4)$$

$$y_{ab} = G_a(f)e^{j\left[\pi\left(1-\frac{2N(f-f_0)}{f_0}\right)\right]} \quad (5)$$

$$H(f) = V_L/V_{IN} = \frac{y_{ab}R_L}{(1 + y_{aa}R_s)(1 + y_{bb}R_L) - {y_{ab}}^2 R_s R_L} \quad (6)$$

Here G_{0m}, θ_m, α, y_{aa}, y_{ab}, y_{ba}, y_{bb}, and $G_a(f)$ are characteristic admittance of the metalized region, transit angle for the metalized strip, a constant to reflect losses due to the internal resonances, input admittance, output admittance, input-to-output short circuit transfer admittance, output-to-input admittance, and conductance, respectively, and ${Y_{11}}^f$ and ${Y_{12}}^f$ are the elements of the acoustic submatrix of the entire IDT. The detailed derivations can be found in our previous publication [10].

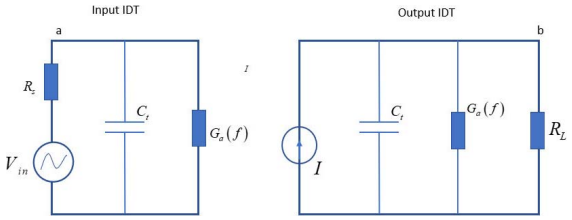

Figure 3. Input and output equivalent circuit for a SAW delay line.

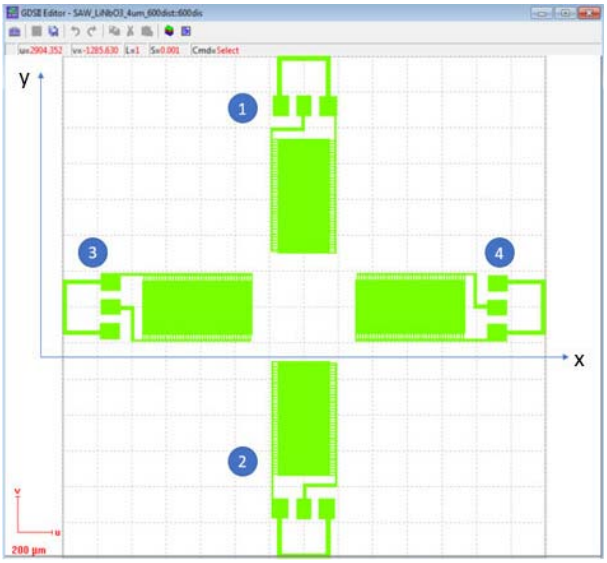

Figure 4. Design of the SAW device (GDS II form).

3. Experiment

In the following experiment, we fabricated SAW devices with different IDT materials: Cu, Al, Cr, and a Ti/Au combination. Titanium is used as an adhesive

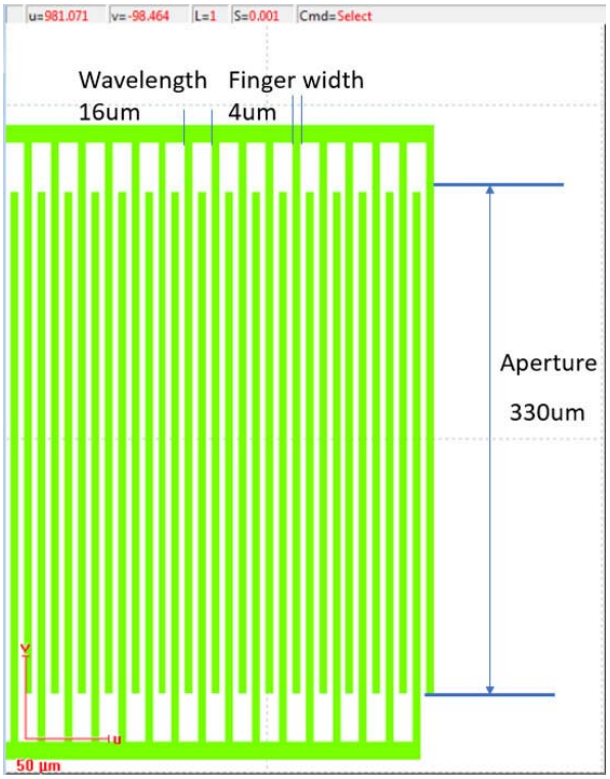

Figure 5. Zoom-in design of the IDTs.

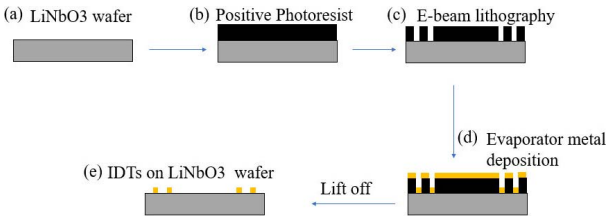

Figure 6. Fabrication steps. (a) Prepare a clean $LiNbO_3$ wafer. (b) Deposit positive photoresist polymethyl methacrylate A4. (c) Electron beam lithography and development. (d) Deposit metal on the wafer using plasma-enhanced chemical vapor deposition. (e) Lift off.

layer that conglutinates Au IDTs with $LiNbO_3$ substrate. The transmission properties of these devices are measured after fabrication.

To reduce the environmental impact, all experiments were implemented at the same location and the same temperature (20°C) and with the same measurement instruments. This work implemented all the fabrication and measurements on one Y-X cut $LiNbO_3$ wafer. In addition, to make the experimental results more reliable, we repeated the measurement by measuring the average transmission property S_{21} and center frequency f_0 of four pairs of SAW devices of the same design. The design of the SAW device is shown in Figure 4. Note that the IDTs are fabricated in four directions because the piezoelectric coefficients and acoustic velocity are different in different directions (along the x-axis and the y-axis in Figure 4). To better explain our design and measurements, IDTs 1 and 2 in Figure 4 are defined as SAW devices parallel to the y-axis. IDTs 3 and 4 are defined as SAW devices parallel to the x-axis.

The zoom-in design of the IDTs is shown in Figure 5. The finger width of IDTs is 4 μm, as is the space between two fingers. The aperture is 330 μm, which is 20 times larger than the wavelength so that it guarantees the generation of the SAW. Figure 6 shows the fabrication process of SAW devices.

4. Results and Discussion

Figure 7 shows a typical transmission property measurement result from a Hewlett Packard Network Analyzer 8722D. The RF probe is an ACP Probe from Cascade Microtech. For example, one of the experiments used the IDT material Au/Ti, which is 195 nm Au on top of 5 nm Ti. Ti of 5 nm is used as an adhesive layer. Figure 7a shows the measurement of the Au/Ti SAW device fabricated parallel to the x-axis (IDTs 3 and 4). The average S_{21} of this SAW device is –41.89 dB, and the center frequency f_0 is 233 MHz. In Figure 7b, by doing the same measurement, the S_{21} and center frequency f_0 of this Au/Ti SAW device fabricated parallel to the y-axis (IDTs 1 and 2) are –47.23 dB and 220 MHz, respectively.

For the IDT materials in this experiment, we used 195 nm Au/5 nm Ti, 200 nm Al, 200 nm Cu, and 200 nm Cr. Table 1 shows the measurement results from Network Analyzer. The data for the resistivity of

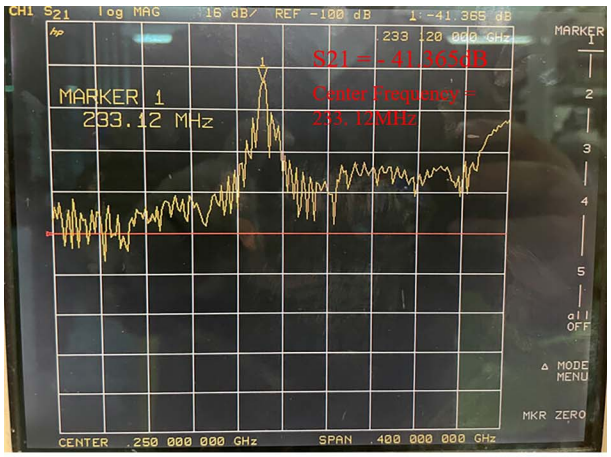

(a)

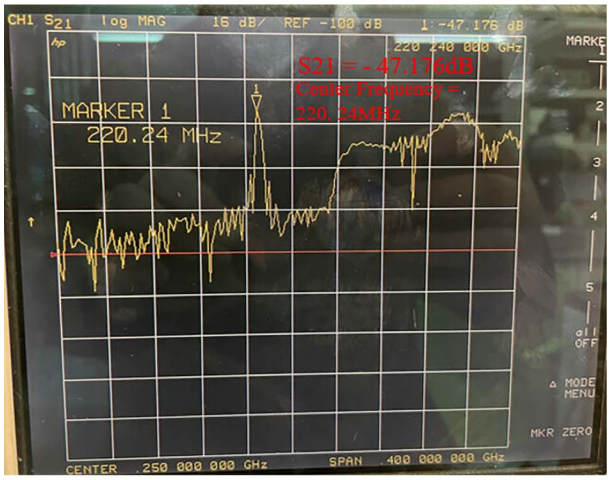

(b)

Figure 7. Measured transmission property of (a) a SAW device fabricated parallel to the x-axis (IDTs 3 and 4) and (b) a SAW device fabricated parallel to the y-axis (IDTs 1 and 2).

different metals at 20°C can be obtained from website of electronic notes https://www.electronics-notes.com/articles/basic_concepts/resistance/electrical-resistivity-table-materials.php.

From Table 1, it can be concluded that lower-resistivity IDT material, such as Cu, results in a reduced insertion loss. The center frequency also shifts with

Table 1. Transmission property of the SAW device with different IDT materials.

			SAW device fabricated parallel to X axis	
IDT Material	Resistivity at 20 °C	Thickness	S21	Center frequency
Cu	16.8 nΩ·m	200nm	-37.86dB	239 MHz
Au /Ti	24.4 nΩ·m/420 nΩ·m	195nm/5nm	-41.36dB	233 MHz
Al	26.5 nΩ·m	200nm	-42.48dB	242 MHz
Cr	129 nΩ·m	200nm	-64.96dB	248 MHz
			SAW device fabricated parallel to Y axis	
IDT Material	Resistivity at 20 °C	Thickness	S21	Center frequency
Cu	16.8 nΩ·m	200nm	-45.82dB	224 MHz
Au /Ti	24.4 nΩ·m/420 nΩ·m	195nm/5nm	-47.18dB	220 MHz
Al	26.5 nΩ·m	200nm	-47.43dB	227 MHz
Cr	129 nΩ·m	200nm	-69.54dB	230 MHz

different IDT materials according to the measurement. The f_0 is 249.75 MHz if no metal is fabricated on the substrate. The frequency shifts of Cu, Au/Ti, Al, and Cr based on the SAW device are 4%, 6.7%, 3.1%, and 0.7%, respectively. The center frequency shifts because the acoustic velocity in the piezoelectric substrate $LiNbO_3$ is affected by the IDTs, caused by the effect of finger reflections, which are due to the high metallization h/λ ratio. Based on (1), when the wavelength is a fixed value, the center frequency increases as the acoustic velocity increases. From the results, we know that the IDT material with lower resistivity on the piezoelectric substrate can cause more frequency shift, meaning that lower-resistivity IDT material can cause more acoustic velocity change.

However, this center frequency change does not work for the Au/Ti combination of IDTs because this complex combination of Au and Ti causes a slight change in shape of the IDT fingers. The metal deposition process was done by using the CHA Industries Criterion Electron Beam Evaporator, which heated and cooled down the environment during fabrication. Unlike other SAW devices using only one metal material, the Au/Ti combination experienced the heating and cooling process twice, causing the shape change of the IDT fingers. The final fabricated IDT fingers of the Au/Ti combination is 5% larger than that of other materials we observed under scanning electron microscopy. In conclusion, with different IDT materials, the center frequency of SAW devices shifts slightly. On the other hand, it is clear that the IDT material can significantly affect the insertion loss of SAW devices because of its effect on the propagation of SAW as discussed above.

5. References

1. C. Gruber, A. Binder, and M. Lenzhofer, "Fast Phase Analysis of SAW Delay Lines," Internet of Things, IoT Infrastructures, Rome, Italy, October 27–29, 2015.
2. D. Chernenko, M. Zhovnir, B. Tsyganok, and O. Oliinyk, "Wireless Passive Pressure Sensor Using Frequency Coded SAW Structures," 2012 35th International Spring Seminar on Electronics Technology, Bad Aussee, Austria, May 9–13, 2012.
3. K. Lee, W. Wang, T. Kim, and S. Yang, "A Novel 440 MHz Wireless SAW Microsensor Integrated With Pressure-Temperature Sensors and ID Tag," *Journal of Micromechanics and Microengineering*, **17**, 3, February 2007, pp. 515-523.
4. J. Luo et al., "A New Type of Glucose Biosensor Based on the Surface Acoustic Wave Resonator Using Mn-Doped ZnO Multilayer Structure," *Biosensors and Bioelectronics*, **49**, 15, November 2013, pp. 512-518.
5. B. Dong, A. Afanasev, R. Johnson, and M. Zaghloul, "Enhancement of Photoemission on p-Type GaAs Using Surface Acoustic Waves," *Sensors*, **20**, 8, April 2020, p. 2419.
6. B. Dong and M. Zaghloul, "Generation and Enhancement of Surface Acoustic Waves on a Highly Doped p-type GaAs Substrate," *Nanoscale Advances*, **1**, July 2019, pp. 3537-3546.
7. F. Guo et al., "Controlling Cell-Cell Interactions Using Surface Acoustic Waves," *Proceedings of the National Academy of Sciences of United States of America*, **112**, 1, January 2015, pp. 43-48.
8. Y. Zhou, *Design and Simulation of SAW-Driven Drug Delivery Device*, Master's thesis, George Washington University, Washington, DC, USA, 2000.
9. P. Delsing et al., "The 2019 Surface Acoustic Waves Roadmap," *Journal of Physics D: Applied Physics*, **52**, 35, July 2019, p. 353001.
10. O. Tigli and M. Zaghloul, "A Novel Saw Device in CMOS: Design, Modeling, and Fabrication," *IEEE Sensors Journal*, **7**, 2, February 2007, pp. 219-227.
11. K. M. Lakin, "Electrode Resistance Effect in Interdigital Transducers," *IEEE Transactions on Microwave Theory and Techniques*, **22**, 4, April 1974, pp. 418-424.
12. C. C. W. Ruppel, W. Ruile, G. Scholl, K. C. Wagner, and O. Manner, "Review of Models for Low-Loss Filter Design and Applications," 1994 Proceeding of IEEE Ultrasonics Symposium, Cannes, France, October 31–November 3, 1994.